THE JOURNAL OF BIOLOGICAL CHEMISTRY VOL. 285, NO. 49, pp. 38692–38699, December 3, 2010
© 2010 by The American Society for Biochemistry and Molecular Biology, Inc. Printed in the U.S.A.

# Aggregation of Detergent-insoluble Tau Is Involved in Neuronal Loss but Not in Synaptic Loss*[S]

Received for publication, April 21, 2010, and in revised form, September 1, 2010 Published, JBC Papers in Press, October 4, 2010, DOI 10.1074/jbc.M110.136630

**Tetsuya Kimura, Tetsuya Fukuda, Naruhiko Sahara, Shunji Yamashita, Miyuki Murayama, Tatsuya Mizoroki, Yuji Yoshiike, Boyoung Lee, Ioannis Sotiropoulos, Sumihiro Maeda, and Akihiko Takashima**[1]

*From the Laboratory for Alzheimer's Disease, Brain Science Institute, Riken, 2-1 Hirosawa, Wako, Saitama 351-0198, Japan*

**Neurofibrillary tangles (NFTs), which consist of highly phosphorylated tau, are hallmarks of neurodegenerative diseases including Alzheimer disease (AD). In neurodegenerative diseases, neuronal dysfunction due to neuronal loss and synaptic loss accompanies NFT formation, suggesting that a process associated with NFT formation may be involved in neuronal dysfunction. To clarify the relationship between the tau aggregation process and synapse and neuronal loss, we compared two lines of mice expressing human tau with or without an aggregation-prone P301L mutation. P301L tau transgenic (Tg) mice exhibited neuronal loss and produced sarcosyl-insoluble tau in old age but did not exhibit synaptic loss and memory impairment. By contrast, wild-type tau Tg mice neither exhibited neuronal loss nor produced sarcosyl-insoluble tau but did exhibit synaptic loss and memory impairment. Moreover, P301L tau was less phosphorylated than wild-type tau, suggesting that the tau phosphorylation state is involved in synaptic loss, whereas the tau aggregation state is involved in neuronal loss. Finally, increasing concentrations of insoluble tau aggregates leads to the formation of fibrillar tau, which causes NFTs to form.**

NFTs[2] are commonly observed in neurodegenerative disorders. Brain regions containing NFTs also exhibit neuronal loss. The rate of neuron loss is much greater than the rate of NFT formation, suggesting that NFT formation and neuronal death share a common mechanism (1, 2). This hypothesis is strongly supported by the discovery of tau gene mutations in individuals with frontotemporal dementia with parkinsonism linked to chromosome 17 (FTDP-17) (3, 4). A single tau gene mutation induces NFT formation and neuronal loss with 100% penetration. Moreover, overexpression of human FTDP-17 tau induces NFT formation, neuronal loss, and behavioral deficits in mice (5–12).

Mice that overexpress P301L mutant tau under the regulation of a tetracycline-inducible promoter display age-related NFTs, neuronal death, and behavioral deficits (13, 14). Although inhibiting mutant tau overexpression in these mice blocks neuronal death and improves memory, NFTs continue to form (13, 15). This suggests that NFTs are not themselves toxic but, instead, that NFT formation and neuronal death and neuronal dysfunction share a common underlying mechanism.

The P301L tau mutation is known as an "aggregation-prone mutation" in that individuals harboring this mutation produce mutant tau that readily aggregates (16–18). The NFTs of one patient with an aggressive FTDP-17 phenotype consisted of only P301L mutant tau (19), indicating that P301L mutant tau itself may possess a toxic function by forming aggregated tau.

The formation of tau fibrils is believed to involve three sequential steps (20, 21). First, monomeric tau binds together to form oligomers that are soluble in sarcosyl solution. The structure of these oligomers, however, is not discernible under atomic force microscopy. Second, as soluble tau oligomers take on a $\beta$-sheet structure, they form tau aggregates that are insoluble in sarcosyl solution. These aggregates become granular-shaped oligomers consisting of ~40 tau molecules that are detectable under atomic force microscopy. Third, increasing concentrations of granular tau oligomer cause the oligomers to fuse to each other to form tau fibrils.

Prefrontal cortex displaying Braak stage I pathology shows significantly higher levels of granular tau oligomer formation than that displaying Braak stage 0 pathology (22), indicating that before NFTs form, tau initiates the formation of different types of aggregates that may play a role in neuronal death and neuronal dysfunction.

In the present study, to understand the role of tau aggregation in neuronal death and neuronal dysfunction, we assessed and compared neuronal death, NFT formation, tau phosphorylation state, synapse number, and behavior in mice that express P301L mutant tau and compared these with mice that express human wild-type tau. The same type of promoter was used to drive tau expression in both lines of mice.

## EXPERIMENTAL PROCEDURES

*Animals*—Generation of Tg mouse lines expressing P301L mutant human tau was performed as described (23). A cDNA construct of P301L mutant human tau was inserted into a CaM kinase II chain expression vector at XhoI sites. A 4.3-kb BglII-NaeI fragment containing the CaM kinase II promoter-P301L mutant human tau cDNA and a 3′-untranslated se-

* This work supported in part by a grant-in-aid for Scientific Research on Priority Areas (Research on Pathomechanisms on Brain Disorders) from the Ministry of Education, Culture, Sports, Science, and Technology of Japan.

[S] The on-line version of this article (available at http://www.jbc.org) contains supplemental Fig. 1.

[1] To whom correspondence should be addressed. Tel.: 81-48-467-9627; Fax: 81-48-467-5916; Email: kenneth@brain.riken.jp.

[2] The abbreviations used are: NFT, neurofibrillary tangles; FTDP-17, frontotemporal dementia with parkinsonism linked to chromosome 17; CaM, calmodulin; TA, temporal area; BLA, basolateral amygdala; LA, lateral amygdala; EC, entorhinal cortex; Tg, transgenic.

quence were used as the transgenes to create the P301Ltau-Tg mice on a C57BL/6J background.

*Antibodies*—For immunohistochemistry and immunoblotting, we used the following antibodies: rabbit polyclonal anti-tau JM; phosphorylation-independent monoclonal anti-tau TauN; phosphorylation-dependent mouse monoclonal anti-tau AT180 (Innogenetics Zwijndrecht, Belgium), which recognizes tau phosphorylated at Thr-231; AT8 (Innogenetics Zwijndrecht), which recognizes tau phosphorylated at Ser-199, Ser-202, and Thr-205; PHF1 (generously provided by Dr. Peter Davies, Albert Einstein College of Medicine, NY), which recognizes tau phosphorylated at Ser-396 and Ser-404; dephosphorylation-dependent mouse monoclonal anti-tau Tau1, which recognizes tau-dephosphorylated Ser-199 and Ser-202; phosphorylation-dependent rabbit polyclonal anti-tau Thr(P)-205, Thr(P)-212, Ser(P)-396, Ser(P)-400, Ser(P)-404, and Ser(P)-422, which recognize tau phosphorylated at Thr-205, Thr-212, Ser-396, Ser-400, Ser-404, and Ser-422, respectively.

*Western Blotting*—Mouse brains were homogenized in Tris-buffered saline (TBS; 10 mM Tris, 150 mM NaCl, pH 7.4) containing protease inhibitors (1 $\mu$g/ml antipine, 5 $\mu$g/ml pepstatin, 5 $\mu$g/ml leupeptin, 2 $\mu$g/ml aprotinin, 0.5 $\mu$M 4-(2-aminoethyl)benzenesulfonyl fluoride hydrochloride), and phosphatase inhibitors (1 mM NaF, 0.4 mM $Na_3VO_4$, and 0.5 mM okadaic acid). After centrifugation at 100,000 $\times$ *g* for 20 min, the supernatant was collected. Sarcosyl-insoluble, paired helical filament-enriched fractions were prepared from TBS-insoluble pellets according to the procedure developed by Greenberg and Davies (24). The resulting precipitate was rehomogenized in 5 volumes of 0.8 M NaCl and 10% sucrose solution and centrifuged at 100,000 $\times$ *g* for 20 min. A one-tenth volume of 10% sarcosyl solution was added to the supernatant, which was then mixed by vortex, incubated for 1 h at 37 °C, and centrifuged at 150,000 $\times$ *g* for 1 h. The resulting pellet was analyzed as the sarcosyl-insoluble fraction. TBS-soluble and sarcosyl-insoluble materials were solubilized in Laemmli sample buffer and subjected to SDS-PAGE. Separated proteins were blotted onto Immobilon-P membranes (Millipore). The membranes were incubated with primary antibody followed by the appropriate-species HRP-conjugated secondary antibody. Chemiluminescent detection (ECL, Amersham Biosciences) was used for visualization. Quantitation and visual analysis of immunoreactivity were performed with a computer-linked LAS-3000 Bio-Imaging Analyzer System (Fujifilm).

*Histology and Immunohistochemical Procedures*—Mice were deeply anesthetized with pentobarbital (50 mg/kg), then transcardially perfused with 10% formalin. Brains were post-fixed in the same fixative for 16 h and embedded in paraffin and sectioned (4–6 $\mu$m) in the coronal plane. Deparaffinized sections were treated with Target Retrieval Solution (Dako) for 20 min at 80 °C, blocked in 0.1% BSA/TBS, and incubated with primary antibodies in 0.1% BSA/TBS overnight at 4 °C. A fluorescent microscope equipped with a cooled CCD camera and Neurolucida software (Version 7; MicroBrightField Inc., Williston, VT) were used to analyze the sections and for acquisition of images under virtual slice mode. NFTs were identified by means of the standard Gallyas silver-impregnation method (10).

For immunostaining of PSD95, deparaffinized coronal sections were treated with proteinase K solution (100 $\mu$M in PBS) for 10 min at 37 °C and incubated with anti-PSD95 antibody. PSD95 immunoreactivity in layer I of the left and right visual cortex and layer I of lateral entorhinal cortex (4.2–4.5 mm posterior to bregma) were quantitated with a fluorescence microscope equipped with a cooled CCD camera and Neurolucida software (Version 7; MicroBrightField Inc., Williston, VT). Quantitative results were presented as normalized intensity values that were determined by dividing fluorescence intensity of entorhinal layer I by that of ipsilateral visual cortex.

*Stereological Analysis*—We estimated neuronal density in the temporal neocortex (TA), lateral entorhinal cortex (EC), lateral amygdala (LA), and basolateral amygdala (BLA) by counting neurons in each area of serial coronal brain sections obtained from three Wtau-Tg mice (male, 23 months old) and three P301Ltau-Tg mice (male, 22 months old). Each section was stained with cresyl violet and examined with a microscope linked to a Neurolucida tracing system. In the present study, due to variations in the structural complexity of the regions of interest, the strategy we selected for estimating neuronal density was to measure the mean number of neurons located within 100-$\mu m^2$ counting boxes covering all neurons within each region of interest. Each region of interest was selected and delineated by an expert in mouse brain cytoarchitectonics (Dr. T. Fukuda), and neuronal counting was performed using the Neurolucida system by researchers who were blind to identifying information about the sections (*e.g.* source animals, age of animals, etc.). For the amygdala, we analyzed sections that were about 50 $\mu$m apart, and for the cortices, we analyzed sections that were 300 $\mu$m apart (three sections containing each region from each animal were analyzed).

*Morris Water Maze Test*—To assess place learning and memory performance of P301Ltau-Tg mice, we used a cylindrical test apparatus (1 m in diameter) and task-fashioned after the Morris water maze. The water was maintained at 24 °C, and the maze was surrounded by landmark objects placed in the room. A slightly submerged transparent platform to which the mice could escape was hidden from view by making the water opaque with a white bio-safe material. The position of the platform was fixed during a 60-s test period.

Mouse behavior and swimming paths during the water maze test were monitored and recorded by a CCD camera mounted overhead; digital data of real-time images were recorded to a PC using the public domain NIH Image program (developed at The United States National Institutes of Health and available on the Internet at rsb.info.nih.gov/nih). Images of the mouse were sampled at 2 Hz. Data were analyzed using customized software based on Matlab (Version 7.2, Mathworks Co. Ltd., Natick, MA) with image analysis tool box (Mathworks Co. Ltd.). During testing, the sequential position of the mouse was determined in each video frame, and the swimming speed, distance from the platform, and latency to reach the platform were calculated. To assess learning, we measured the distance between the mouse and the platform

every 0.5 s until the mouse reached the platform. Next, we calculated the total distance traveled by the mouse by integrating the distance between the mouse and the platform. This "integral distance" value represents the error score. We used this error score as a measure of learning performance.

For learning trials, the mouse was gently placed on the water surface close to the cylinder wall in the opposite half of the maze away from the platform; it was allowed to swim freely for a 60-s test period. When the mouse did not escape to the submerged platform within this test period, we gently navigated it to the platform by hand and made it stay there for 20 s. For each mouse, we carried out three learning trials per day for nine successive days. A single probe test was given on the 10th day in which the platform was removed from the maze in the absence of the mouse . The mouse was introduced into the maze as before and allowed to search for the missing platform for 60 s.

An error score for the probe test was calculated by measuring the total distance the mouse traveled for 60 s. Statistical analyses were conducted using PRISM4 (GraphPad Software Inc., La Jolla CA). Data were analyzed using the Friedman test or two-way analysis of variance unless noted otherwise. If a mouse remembered the location of the platform during training, its probe score (error score per frame) was small, because the mouse spent most of its time searching the area where the platform was formerly located.

## RESULTS

*Expression of P301L Mutant Tau in Mouse Brain*—CaM kinase II promoter regulated the expression of P301L mutant human 4 repeat tau in P301Ltau-Tg mice (Fig. 1*A*); CaM kinase II promoter also regulated the expression of wild-type tau in Wtau-Tg mice. The pattern of tau expression in different brain regions was determined by immunoblotting using TauN antibody (Fig. 1*B*), which recognizes the N terminus of tau. Cerebral cortex, hippocampus, and striatum showed the highest levels of P301L mutant human 4 repeat tau expression, 3–5-fold greater than that of endogenous tau. Thalamus, olfactory bulb, and midbrain had moderate levels, whereas in medulla, cerebellum, and spinal cord, expression of P301L mutant human 4 repeat tau was not detected. There were no differences in the expression patterns between male and female mice or between young and old mice. Wild-type and mutant human tau expression patterns in P301Ltau-Tg and Wtau-Tg mice were the same; however, P301Ltau-Tg mice had about 1.8-fold more human tau in cerebral cortex, hippocampus, entorhinal cortex, and striatum than Wtau-Tg mice.

*Less Phosphorylation and Greater Insolubility of P301L Tau*—To assess tau phosphorylation state and aggregation, we prepared P301Ltau-Tg mouse brain (hippocampus) homogenates in TBS and analyzed tau in the soluble fraction. We previously observed that Wtau-Tg mice show age-dependent increases in tau phosphorylation (23); thus, in the present study, we compared the tau phosphorylation state in old P301Ltau-Tg mice and old Wtau-Tg mice (Fig. 2*A*). Although the phosphorylation-independent tau antibody TauN prominently labeled the faster mobility human tau band derived

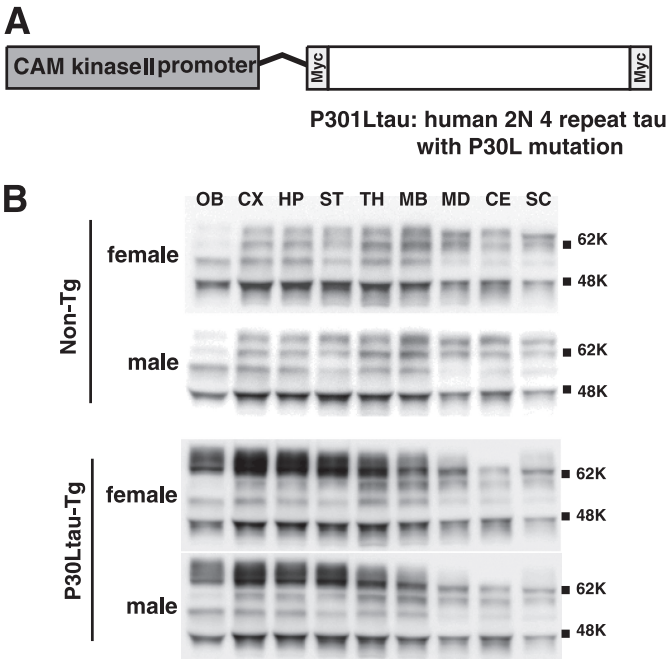


FIGURE 1. **Generation of a transgenic mouse expressing P301L mutant human 2N/4 repeat tau.** *A,* a diagram shows that the expression of mutant P301L human 4 repeat tau tagged with myc and FLAG epitopes was regulated by the CaM kinase II promoter. *B*, Western blots show the pattern of tau expression in different brain regions. Blots were probed with anti-tauN antibody, which recognizes the N terminus of tau. Male and female mice did not exhibit different expression patterns. *OB*, olfactory bulb; *CE*, cerebellum; *CX*, cerebral cortex; *HP*, hippocampus; *MB*, midbrain; *SC*, spinal cord; *ST*, striatum; *TH*, thalamus; *MD*, medulla.

from P301Ltau-Tg samples (*filled arrowheads*), it also labeled the slower mobility human tau band derived from Wtau-Tg samples (*open arrowheads*), suggesting that P301L mutant tau in the brains of aged mice may be less phosphorylated than wild-type human tau.

Next, we analyzed the phosphorylation state of individual sites on tau using different phosphorylation-dependent tau antibodies. Tau1, a dephosphorylation-dependent anti-tau antibody, primarily labeled the faster mobility human tau band from Wtau-Tg and P301Ltau-Tg samples. However, normalized tau immunoreactivity (normalized to TauN immunoreactivity) was significantly greater in samples derived from P301Ltau-Tg mice than in those from Wtau-Tg mice. AT8, which recognizes tau phosphorylated at Ser-199, Ser-202, and Thr-205, anti-Thr(P)-205 antibody, which recognizes tau phosphorylated at Thr-205, and anti-Thr(P)-212 antibody, which recognizes tau phosphorylated at Thr-212, labeled the slower mobility human tau band from Wtau-Tg and P301Ltau-Tg samples. Band intensities were normalized by the intensity of the TauN band (Fig. 2*A*, *left panel*). Normalized immunoreactivities of Thr(P)-205- and Thr(P)-212-immunoreactive human tau bands were significantly lower in P301Ltau-Tg than in Wtau-Tg samples. AT8 also showed the same tendency, although it was not statistically significant at $p < 0.05$. AT180, which recognizes tau phosphorylated at Thr-231, primarily labeled the slower mobility human tau band from both Tg mouse line samples; there was no difference in the normalized AT180 immunoreactivity between samples from Wtau-Tg and P301Ltau-Tg mice. Ser(P)-396,

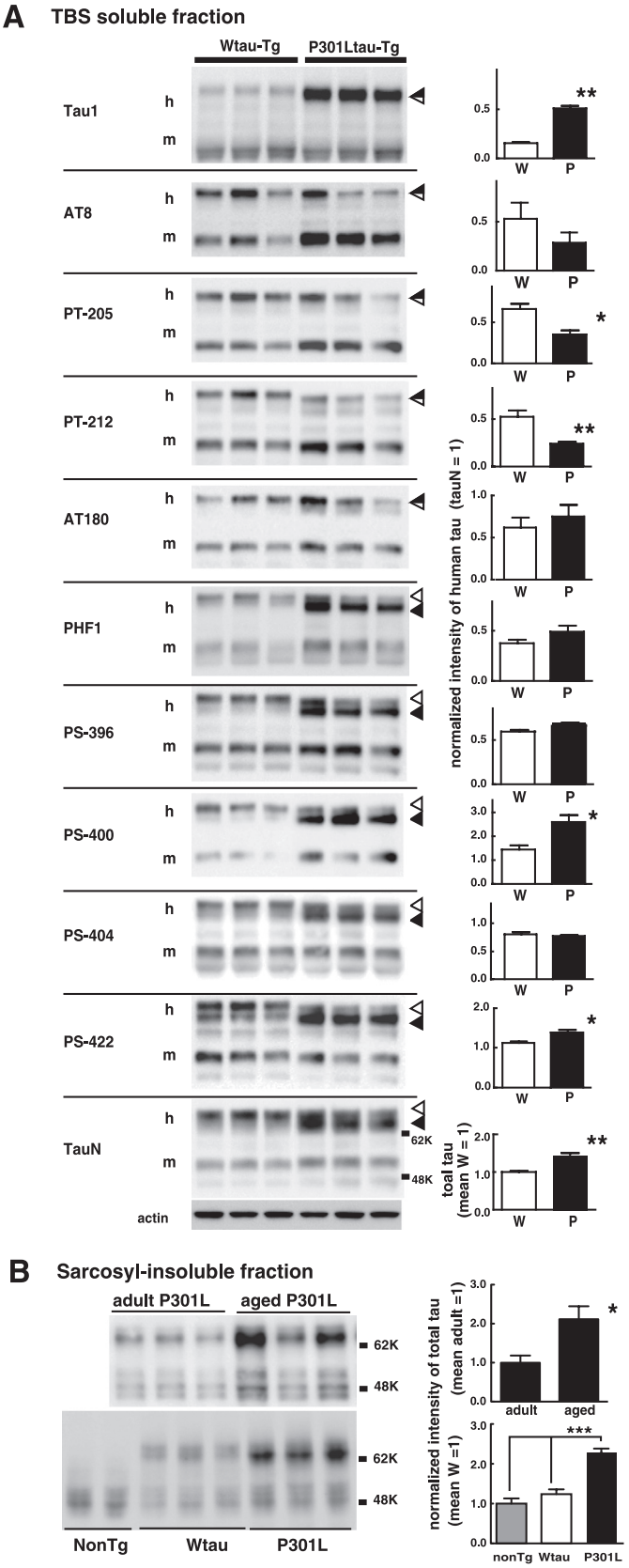


FIGURE 2. **The brains of P301L-Tg mice form sarcosyl-insoluble tau aggregates, but tau from P301L-Tg mice is less phosphorylated than that from Wtau-Tg mice.** *A*, Western blots of TBS-soluble fractions from the brain homogenates of 22-month-old P301Ltau-Tg mice and 22-month-old Wtau-Tg mice (*left panel*) and histograms show the corresponding tau intensity levels normalized according to TauN immunoreactivity (*right panel*; *W*, Wtau-Tg mice; *P*, P301Ltau-Tg mice). The immunoblots were probed with various anti-tau antibodies, as indicated. Anti-Thr(P)-205, anti-Thr(P)-212, anti-Ser(P)-396, anti-Ser(P)-400, and anti-Ser(P)-422 recognize tau phosphorylated at Thr-205, Thr-212, Ser-396, Ser-400, Ser-404, and Ser-422, respectively. TauN recognizes total phosphorylation-independent tau; AT8 recognizes tau phosphorylated at Ser-199, Ser-202, and Thr-205; AT180 recognizes tau phosphorylated at Thr-231; PHF1 recognizes tau phosphorylated at Ser-396 and Ser-404; actin is shown as an internal control. *Open arrowheads* indicate the mobility of wild-type human tau bands; *filled arrowheads* indicate the mobility of the P301L human tau bands. Data are represented as the averages ± S.E. *, $p < 0.05$ (Mann-Whitney test); **, $p < 0.01$ (Mann-Whitney test). *B*, *upper left panel*, Western blots of sarcosyl-insoluble fractions from the brain homogenates of 10-month-old P301Ltau-Tg mice (adult) and 22-month-old P301Ltau-Tg mice (aged) are shown. Immunoreactivities were quantified and represented as averages ± S.E. ($n = 5$). *, $p < 0.05$ (Mann-Whitney test) (*upper right panel*), *Lower panel*, Western blots are shown of sarcosyl-insoluble fractions from the brain homogenates of aged (22–24 months old) non-Tg, Wtau-Tg, and P301Ltau-Tg mice. Immunoreactivities were quantified and are represented as averages ± S.E. ($n = 5$). *, $p < 0.05$; ***, $p < 0.005$ (Mann-Whitney test) (*lower right panel*). Immunoreactivities of sarcosyl-insoluble tau in Wtau-Tg mice were similar to levels in non-Tg mice.

which recognizes tau phosphorylated at Ser-396, and Ser(P)-404, which recognizes tau phosphorylated at Ser-404, primarily labeled the faster mobility human tau band derived from P301Ltau-Tg samples but primarily labeled the slower human tau band derived from Wtau-Tg samples. Normalized immunoreactivities of Ser(P)-396 and Ser(P)-404 did not significantly differ between P301Ltau-Tg and Wtau-Tg mice; PHF1 immunoreactivity also did not differ between P301Ltau-Tg and Wtau-Tg mice. Anti-Ser(P)-400, which recognizes tau phosphorylated at Ser-404, and anti-Ser(P)-422, which recognizes tau phosphorylated at Ser-422, primarily labeled the faster mobility human tau band derived from P301Ltau-Tg samples but primarily labeled the slower human tau band derived from Wtau-Tg samples. Normalized immunoreactivities for both antibodies were significantly greater in P301Ltau-Tg than in Wtau-Tg mice.

In general, P301L mutant human tau tended to be less phosphorylated in its N terminus projection region but more phosphorylated in its C terminus compared with wild-type human tau. All phosphorylation-dependent antibodies recognized the slower mobility band from Wtau-Tg samples. With respect to P301Ltau-Tg samples, however, phosphorylation-dependent antibodies recognizing the C terminus region labeled the faster mobility tau band, whereas phosphorylation-dependent antibodies recognizing the N terminus projection region labeled the slower mobility tau band. These results suggest that the brains of aged P301Ltau-Tg mice have lower levels of fully phosphorylated tau than the brains of aged Wtau-Tg mice.

In addition to analyzing the P301L tau phosphorylation state in mouse brain, we investigated the solubility of P301L tau in sarcosyl solution (Fig. 2). As previously mentioned, we did not recover human tau in sarcosyl-insoluble fractions derived from the brains of Wtau-Tg mice (10) (Fig. 2*B*, *lower panel*). In the present study, however, we recovered more human tau in the sarcosyl-insoluble fraction derived from the brains of aged P301Ltau-Tg mice with age-dependent manner (Fig. 2*B*, *upper panel*). We also confirmed that P301Ltau-Tg mice have lower levels of fully phosphorylated tau than Wtau-Tg mice. Taken together, these results indicate that,

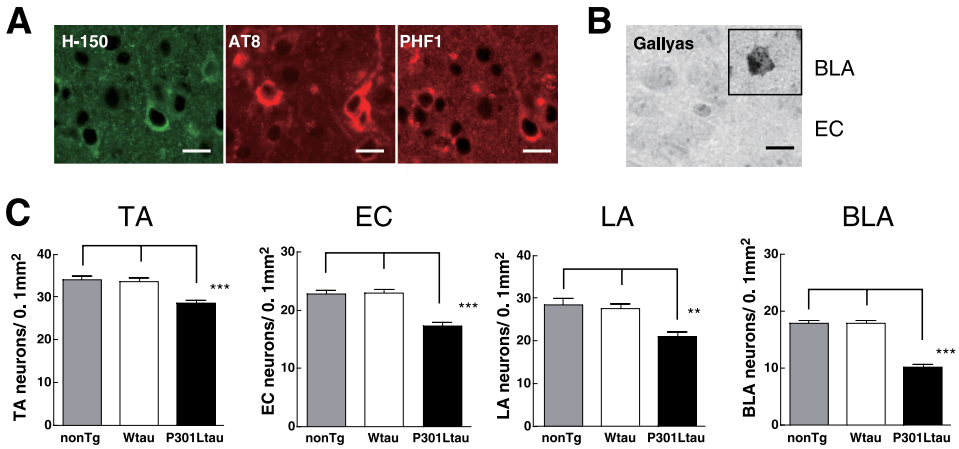


FIGURE 3. **The brains of P301Ltau-Tg mice display neuron loss but not NFTs.** *A,* entorhinal cortex sections immunostained with phosphorylation-independent anti-human tau antibody (H-150) or phosphorylation-dependent anti-tau antibodies (AT8 and PHF1) are shown. Phosphorylated human tau accumulated in cell bodies and dendrites of neurons in the entorhinal cortex. *B,* shown is the entorhinal cortex section stained with the Gallyas silver staining method. No silver-stained neurons were seen in the entorhinal cortex, but silver-stained neurons were occasionally seen in the BLA. *C,* histograms show the numbers of neurons counted in the TA of neocortex (*NC*), EC, LA, and BLA of Non-Tg, Wtau-Tg, and P301Ltau-Tg mice. Three cresyl violet-stained brain sections containing each region were analyzed, and the number of neurons in each region was counted using a Neurolucida system ($n = 3$ mice for each group). For the amygdala, we analyzed sections that were about 50 $\mu$m apart, and for neocortex and entorhinal cortex, we analyzed sections that were 300-$\mu$m apart. Data are represented as the averages ± S.E. *, $p < 0.05$ (Mann-Whitney test); **, $p < 0.01$ (Mann-Whitney test); ***, $p < 0.005$ (Mann-Whitney test). *A* and *B scale bars*, 10 $\mu$m.

although less phosphorylated than wild-type tau, P301L mutant tau could form sarcosyl-insoluble tau aggregates. In other words, P301L tau can form tau aggregates in even less tau phosphorylation states compare with Wtau-Tg mouse.

*P301L tau-Tg Mice Exhibit Neuron Loss but Not NFTs*—To understand how tau aggregation affects NFT formation and neuron loss, we examined P301Ltau-Tg mouse brains using immunohistochemical and silver-staining methods (Fig. 3). Some neurons were immunoreactive for phosphorylation-dependent anti-tau antibodies (Fig. 3*A*). Phosphorylated tau accumulated in cell bodies and dendrites of neurons. Most neurons, however, were negative for Gallyas silver staining (Fig. 3*B*). Only occasional Gallyas-positive neurons were observed in lateral amygdala (Fig. 3*B*, *inset*). Therefore, although phosphorylated tau accumulated in some neurons, NFTs did not form in most neurons.

Next, we assessed the number of neurons in the TA, EC, LA, and BLA of non-Tg, Wtau-Tg, and P301Ltau-Tg mice (Fig. 3*C*). The density of neurons in TA, EC, LA, and BLA of P301Ltau-Tg mice was significantly reduced compared with that of non-Tg and Wtau-Tg mice (Fig. 3*C*). Neuron counts in these areas of Wtau-Tg and non-Tg mice were not significantly different, as previously reported (23) (Fig. 3*C*). P301Ltau-Tg mice had neuron loss in various brain regions that also exhibited sarcosyl-insoluble tau aggregation but no NFTs. These results suggest that an accumulation of sarcosyl-insoluble tau aggregates in the brains of P301Ltau-Tg mice may be involved in neuronal loss, as Wtau-Tg mice displayed neither sarcosyl-insoluble tau nor neuron loss.

*P301L Tau-Tg Mice Lack Behavioral Signs of Brain Dysfunction*—The EC is an important brain region involved in memory. Because P301Ltau-Tg mice exhibited significant neuron loss in the EC, we tested P301Ltau-Tg mice in the Morris Water Maze, a behavioral task that assesses place learning and memory. As shown in Fig. 4*A*, the mean error scores of P301Ltau-Tg mice diminished with repetitive training, as did those of non-Tg mice. Consistent with our previous findings, the mean error scores of Wtau-Tg mice did not, however, decrease (23). In the probe test, P301Ltau-Tg and non-Tg mice remembered the maze quadrant in which the escape platform was located and had significantly lower probe scores than Wtau-Tg mice (Fig. 4*B*). This suggests that the neuron loss in P301Ltau-Tg mice did not affect their ability to form memories.

In a previous report we demonstrated that the EC of Wtau-Tg mice have fewer synapses than non-Tg mice and that this decrease in synapses was associated with memory impairment (23). To determine whether P301Ltau-Tg mice have fewer synapses, we compared immunoreactivity for PSD95, a postsynaptic marker, in brain sections from P301Ltau-Tg, Wtau-Tg, and non-Tg mice (Fig. 4*C*). PSD95 immunoreactivity in the visual cortex (V2) did not differ in non-Tg, Wtau-Tg, and P301Ltau-Tg mice (Fig. 4*C*). PSD95 immunoreactivity in the EC of non-Tg and P301Ltau-Tg mice did not differ significantly (Fig. 4, *C* and *D*). However, PSD95 immunoreactivity in the EC of Wtau-Tg mice was significantly reduced (Fig. 4, *C* and *D*), which was confirmed by synaptophysine immunoreactivity in P301Ltau-Tg, Wtau-Tg, and non-Tg mice (supplemental Fig. 1). These results indicate that the sarcosyl-insoluble tau of P301Ltau-Tg mice may be involved in neuron loss but not in synapse loss. This may explain why P301Ltau-Tg mice retain the ability to form place memories despite exhibiting significant neuronal loss.

## DISCUSSION

*P301L Tau Mutation*—The P301L human tau-overexpressing mouse was generated and showed NFTs and neuronal loss (3, 4). Lines of rTg4510 mice (14) show a 7-fold overexpression of P301L tau relative to endogenous mouse tau and start to display pretangles at 14.5 months of age. By contrast, another line of mice that shows a 13-fold overexpression of P301L tau begins to exhibit argyrophilic NFT-like pathology

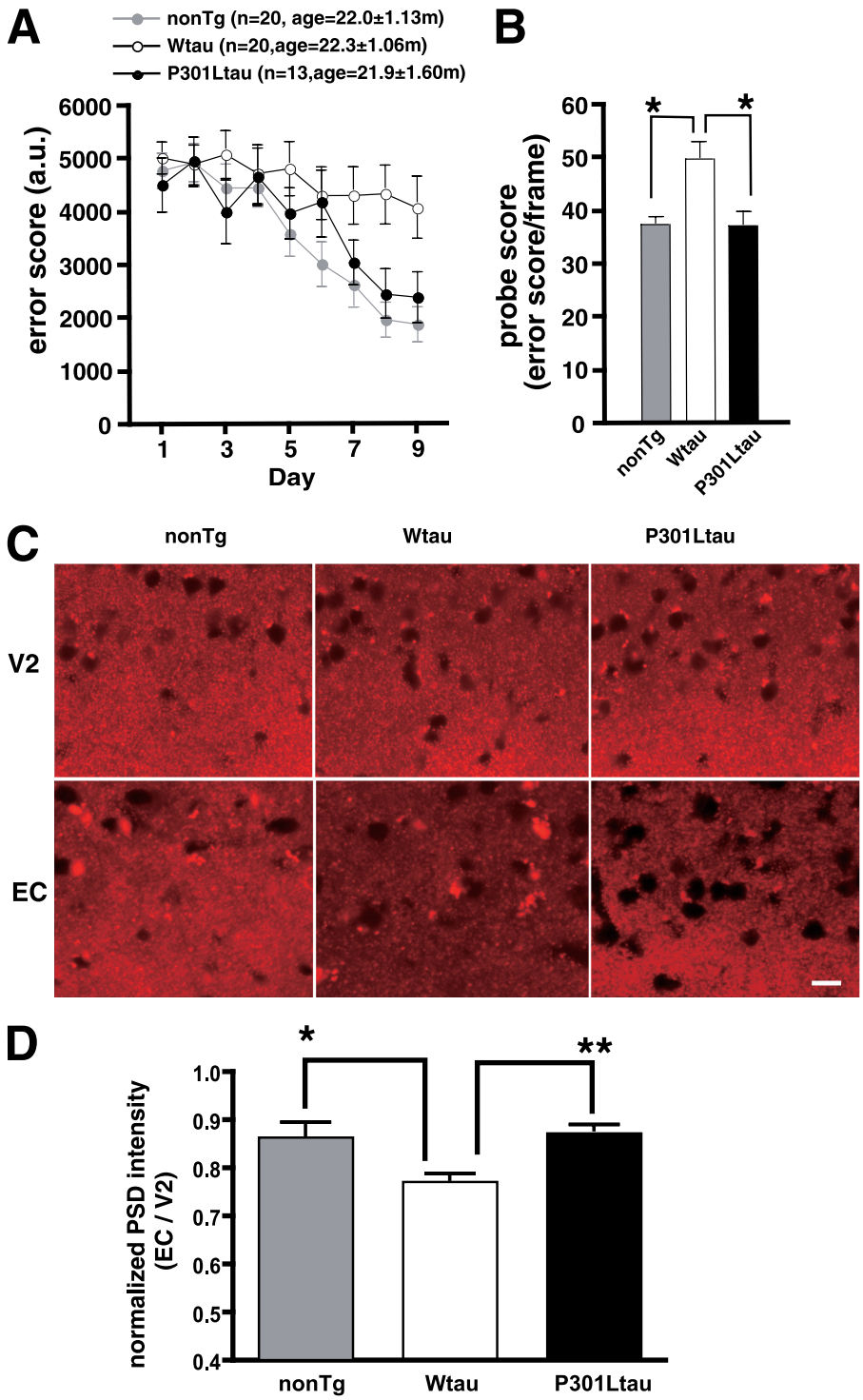


FIGURE 4. **Aged P301Ltau-Tg mice have normal place learning and memory.** The Morris water maze was used to assess the place learning and memory of aged (20–24 months old) non-Tg ($n = 20$), Wtau-Tg ($n = 20$), and P301Ltau-Tg ($n = 13$) mice. *A,* learning and memory performance are expressed as error scores. Learning curves and memory performance of non-Tg and P301Ltau-Tg mice were not significantly different ($p < 0.577$, $F = 0.449$, repeated measures two-way analysis of variance). However, Wtau-Tg mice took significantly longer than non-Tg mice to learn the task ($p < 0.0326$, $F = 4.92$, repeated measures two-way analysis of variance). *a.u.*, arbitrary units. *B,* probe scores of P301Ltau-Tg and non-Tg mice were not different ($p > 0.05$, Dunn's multiple comparison test). However, the probe scores of Wtau-Tg mice were worse than those of non-Tg mice and P301Ltau-Tg mice ($p < 0.05$ for each, Dunn's multiple comparison test). Probe score is a measure of memory performance. *C,* shown are coronal brain sections from non-Tg, Wtau-Tg, and P301Ltau-Tg mice. The sections were immunostained with anti-PSD95 antibody, an antibody against the post-synaptic marker PSD95. Consistent with the learning and memory performance results, PSD95 immunoreactivity in the entorhinal cortex of non-Tg and P301Ltau-Tg mice were not different. However, PSD95 immunoreactivity was reduced in the entorhinal cortex of Wtau-Tg mice. *D*, shown is quantitative analysis of PSD95 immunoreactivity in entorhinal cortex. Results are expressed as fluorescence intensity of layer I of the lateral entorhinal cortex normalized by that of layer I of ipsilateral visual cortex (non-Tg, $n = 7$; Wtau-Tg, $n = 6$; and P301L-Tg, $n = 3$). Measurements were done on coronal brain sections. Dunn's multiple comparison test revealed a significant difference in PSD95 immunoreactivity between Wtau-Tg and P301L-Tg mice ($p < 0.01$). Data are represented as averages ± S.E. *, $p < 0.05$; **, $p < 0.01$. *V2*, visual cortex.

at 5.5 months of age (13). Moreover, the amount of sarcosyl-insoluble tau and the number of NFTs in these mice is correlated. In the present study our P301Ltau-Tg mice showed a 3–5-fold overexpression of P301L tau relative to endogenous mouse tau and formed sarcosyl-insoluble tau with few argyrophilic NFTs at 22 months of age. The differences displayed by these three lines of mice may be due to the varying degrees of P301L tau expression in these mice. On the other hand, our Wtau-Tg mice, expressing 2–3-fold wild human tau relative to endogenous mouse tau, did not form sarcosyl insoluble tau, and the other mouse lines overexpressing 4–15-fold wild human tau relative to endogenous mouse tau have not reported the formation of sarcosyl insoluble tau aggregation (25). The difference between our Wtau- and P301Ltau-Tg shown here may be due not to tau expression levels but to the existence of FTDP-17 mutation.

*Tau Phosphorylation and Aggregation*—The present analysis of P301Ltau-Tg mice suggests that tau with the P301L mutation forms sarcosyl-insoluble tau even though it is less phosphorylated than wild-type tau. These findings are supported by the *in vitro* observations that P301L tau only requires 4–6 mol of phosphate per tau to polymerize into filaments, whereas wild-type tau requires more than 10 mol of phosphate per tau for self-aggregation (26). This is likely due to the fact that tau with the FTDP-17 mutation enhances the formation of local $\beta$-structures (27), which may promote tau aggregation faster than what occurs with wild-type tau. Thus, before becoming hyperphosphorylated, P301L mutant tau can begin to self-aggregate. We also found that P301Ltau was less phosphorylated in mouse brain than wild-type human tau. Phosphorylation state, however, can affect tau conformation. Jeganathan *et al.* (28) reported that tau in solution adopts a "paperclip" conformation. Pseudophosphorylation of either the AT8 site or the PHF1 site causes the paperclip conformation to open up, whereas pseudophosphorylation of both AT8 and PHF1 sites causes tau to form a compact paperclip conformation (28). Additional phosphorylation induces pathological conformational changes (28).

When AT8 sites are pseudo-phosphorylated, the distance between the tau N and C termini is longer than when PHF1 sites or AT8 and PHF1 sites are pseudo-phosphorylated (28). For the latter situations, the distances between the tau C and N termini are similar. In the present study we found that the PHF1 site of P301L tau was phosphorylated to a similar extent as wild-type tau, whereas the AT8 site of P301L tau was phosphorylated to a lesser extent than wild-type tau. This may be because P301L tau could form aggregates before phosphorylation of tau at N-terminal site. Nonetheless, P301L tau formed sarcosyl-insoluble tau aggregates even though it was not fully phosphorylated. If shortening the distance between the C and N termini of tau is the minimum requirement needed for tau to adopt a pathological conformation, phosphorylation of the C-terminal region of P301L tau may be sufficient for it to form a pathological conformation, resulting in the formation of sarcosyl-insoluble tau aggregates. Although aged Wtau-Tg mice formed hyperphosphorylated tau, they did not form insoluble tau aggregates. This may be because hyperphosphorylated tau levels in these mice are lower than those needed for inducing the formation of insoluble tau.

*Tau Aggregation Induces Neuron Loss and NFT Formation*—Although P301Ltau-Tg mice formed sarcosyl-insoluble tau that was accompanied by neuron loss, they did not form Gallyas silver-impregnated NFTs, suggesting that NFT formation and neuron loss might occur through different tau-related mechanisms. This notion is supported by a previous report (14). Thus, an aggregated form of tau included in sarcosyl-insoluble fraction might contribute to neuronal loss. In an *in vitro* tau aggregation system, we have found that the sarcosyl-insoluble fraction contains granular tau oligomers and tau fibrils (22). Because NFTs consist of bundles of tau fibrils, the observation that P301L tau formed sarcosyl-insoluble aggregates in brains without forming NFTs suggests that the neurons of P301Ltau-Tg mice produce large amounts of granular tau oligomers but few fibrils. If this is indeed the case, granular tau oligomer can be considered to be a toxic tau aggregate species.

Shiarli *et al.* (29) compared the differences between FTDP-17 and AD and found that, whereas the tissue loss is greater in FTPD-17, the amount of NFTs is about one-tenth that in AD. This observation suggests that FTDP-17-related mutant tau tends to induce neuronal loss rather than the formation of NFTs. As with FTDP-17 patients, our P301L tau mice tend to display more neuronal loss than NFT formation.

*Tau-induced Synapse Loss and Neuron Loss*—Wtau-Tg mice exhibit memory impairment in the absence of sarcosyl-insoluble tau aggregate formation (23). By contrast, P301Ltau-Tg mice did not exhibit memory impairment even though they exhibited neuron loss and formed sarcosyl-insoluble tau aggregates. The memory impairment disparity between Wtau-Tg and P301Ltau-Tg mice may due to decreased PSD95 immunoreactivity and, hence, fewer synapses in the EC of Wtau-Tg mice (23). The present study demonstrated that PSD95 immunoreactivity in the EC of P301Ltau-Tg mice was comparable with that of Non-Tg mice even though the number of EC neurons in P301Ltau-Tg mice was about 77% that in non-Tg mice. That the number of synapses in P301Ltau-Tg mice was not reduced suggests the remaining neurons sufficiently maintain neuronal function by increasing the number of synapses (30, 31). The observation that P301Ltau-Tg mice display enhanced long term potentiation (32) before NFT formation supports the premise that an increase in the number of synapses may compensate for the reduction in the number of neurons. Indeed, a more than 50% neuron loss in hippocampus could not compensate for neuronal function, as such a loss was found to impair memory formation (14).

In P301Ltau-Tg mice, neuron loss occurred without affecting the number of synapses, whereas in Wtau-Tg mice synapse loss occurred without affecting the number of neurons. Moreover, P301Ltau-Tg mice formed less phosphorylated forms of tau and formed sarcosyl-insoluble tau aggregates, whereas Wtau-Tg mice formed hyperphosphorylated tau but did not form sarcosyl-insoluble tau aggregates. Therefore, the soluble form of hyperphosphorylated tau may be involved in synapse loss, whereas the insoluble form of tau may be in-

volved in neuron loss. During neurodegeneration, tau becomes hyperphosphorylated and forms a very compact paperclip-like structure (33), one that induces synaptic loss. Concurrently, increasing concentrations of hyperphosphorylated tau induce the formation of granular tau oligomers, which are not synaptotoxic but do cause neuronal loss. As the concentration of granular tau oligomers increases, a non-neurotoxic form of tau (fibrillar tau) forms, ultimately leading to the formation of NFTs. Different forms of tau aggregates may be involved in the different pathological features of neurodegeneration.

## REFERENCES


1. Gómez-Isla, T., Hollister, R., West, H., Mui, S., Growdon, J. H., Petersen, R. C., Parisi, J. E., and Hyman, B. T. (1997) *Ann. Neurol.* **41,** 17–24
2. Ingelsson, M., Fukumoto, H., Newell, K. L., Growdon, J. H., Hedley-Whyte, E. T., Frosch, M. P., Albert, M. S., Hyman, B. T., and Irizarry, M. C. (2004) *Neurology* **62,** 925–931
3. Goedert, M., and Spillantini, M. G. (2000) *Biochim. Biophys. Acta* **1502,** 110–121
4. Hutton, M. (2000) *Ann. N.Y. Acad. Sci.* **920,** 63–73
5. Dawson, H. N., Cantillana, V., Chen, L., and Vitek, M. P. (2007) *J. Neurosci.* **27,** 9155–9168
6. Goedert, M., and Jakes, R. (2005) *Biochim. Biophys. Acta* **1739,** 240–250
7. Götz, J., Streffer, J. R., David, D., Schild, A., Hoerndli, F., Pennanen, L., Kurosinski, P., and Chen, F. (2004) *Mol. Psychiatry* **9,** 664–683
8. Lewis, J., McGowan, E., Rockwood, J., Melrose, H., Nacharaju, P., Van Slegtenhorst, M., Gwinn-Hardy, K., Paul Murphy, M., Baker, M., Yu, X., Duff, K., Hardy, J., Corral, A., Lin, W. L., Yen, S. H., Dickson, D. W., Davies, P., and Hutton, M. (2000) *Nat. Genet.* **25,** 402–405
9. Pérez, M., Ribe, E., Rubio, A., Lim, F., Morán, M. A., Ramos, P. G., Ferrer, I., Isla, M. T., and Avila, J. (2005) *Neuroscience* **130,** 339–347
10. Tanemura, K., Akagi, T., Murayama, M., Kikuchi, N., Murayama, O., Hashikawa, T., Yoshiike, Y., Park, J. M., Matsuda, K., Nakao, S., Sun, X., Sato, S., Yamaguchi, H., and Takashima, A. (2001) *Neurobiol. Dis.* **8,** 1036–1045
11. Taniguchi, T., Doe, N., Matsuyama, S., Kitamura, Y., Mori, H., Saito, N., and Tanaka, C. (2005) *FEBS Lett.* **579,** 5704–5712
12. Sato, S., Tatebayashi, Y., Akagi, T., Chui, D. H., Murayama, M., Miyasaka, T., Planel, E., Tanemura, K., Sun, X., Hashikawa, T., Yoshioka, K., Ishiguro, K., and Takashima, A. (2002) *J. Biol. Chem.* **277,** 42060–42065
13. Ramsden, M., Kotilinek, L., Forster, C., Paulson, J., McGowan, E., SantaCruz, K., Guimaraes, A., Yue, M., Lewis, J., Carlson, G., Hutton, M., and Ashe, K. H. (2005) *J. Neurosci.* **25,** 10637–10647
14. Santacruz, K., Lewis, J., Spires, T., Paulson, J., Kotilinek, L., Ingelsson, M., Guimaraes, A., DeTure, M., Ramsden, M., McGowan, E., Forster, C., Yue, M., Orne, J., Janus, C., Mariash, A., Kuskowski, M., Hyman, B., Hutton, M., and Ashe, K. H. (2005) *Science* **309,** 476–481
15. Spires, T. L., Orne, J. D., SantaCruz, K., Pitstick, R., Carlson, G. A., Ashe, K. H., and Hyman, B. T. (2006) *Am. J. Pathol.* **168,** 1598–1607
16. Barghorn, S., Zheng-Fischhöfer, Q., Ackmann, M., Biernat, J., von Bergen, M., Mandelkow, E. M., and Mandelkow, E. (2000) *Biochemistry* **39,** 11714–11721
17. Lee, S., Jung, C., Lee, G., and Hall, G. F. (2009) *J. Alzheimers Dis.* **16,** 99–111
18. Nacharaju, P., Lewis, J., Easson, C., Yen, S., Hackett, J., Hutton, M., and Yen, S. H. (1999) *FEBS Lett.* **447,** 195–199
19. Miyasaka, T., Morishima-Kawashima, M., Ravid, R., Heutink, P., van Swieten, J. C., Nagashima, K., and Ihara, Y. (2001) *Am. J. Pathol.* **158,** 373–379
20. Maeda, S., Sahara, N., Saito, Y., Murayama, M., Yoshiike, Y., Kim, H., Miyasaka, T., Murayama, S., Ikai, A., and Takashima, A. (2007) *Biochemistry* **46,** 3856–3861
21. Kimura, T., Yamashita, S., Nakao, S., Park, J. M., Murayama, M., Mizoroki, T., Yoshiike, Y., Sahara, N., and Takashima, A. (2008) *PLoS ONE* **3,** e3540
22. Maeda, S., Sahara, N., Saito, Y., Murayama, S., Ikai, A., and Takashima, A. (2006) *Neurosci. Res.* **54,** 197–201
23. Kimura, T., Yamashita, S., Fukuda, T., Park, J. M., Murayama, M., Mizoroki, T., Yoshiike, Y., Sahara, N., and Takashima, A. (2007) *EMBO J.* **26,** 5143–5152
24. Greenberg, S. G., and Davies, P. (1990) *Proc. Natl. Acad. Sci. U.S.A.* **87,** 5827–5831
25. Götz, J. (2001) *Brain Res. Brain Res. Rev.* **35,** 266–286
26. Alonso Adel, C., Mederlyova, A., Novak, M., Grundke-Iqbal, I., and Iqbal, K. (2004) *J. Biol. Chem.* **279,** 34873–34881
27. von Bergen, M., Barghorn, S., Li, L., Marx, A., Biernat, J., Mandelkow, E. M., and Mandelkow, E. (2001) *J. Biol. Chem.* **276,** 48165–48174
28. Jeganathan, S., Hascher, A., Chinnathambi, S., Biernat, J., Mandelkow, E. M., and Mandelkow, E. (2008) *J. Biol. Chem.* **283,** 32066–32076
29. Shiarli, A. M., Jennings, R., Shi, J., Bailey, K., Davidson, Y., Tian, J., Bigio, E. H., Ghetti, B., Murrell, J. R., Delisle, M. B., Mirra, S., Crain, B., Zolo, P., Arima, K., Iseki, E., Murayama, S., Kretzschmar, H., Neumann, M., Lippa, C., Halliday, G., Mackenzie, J., Khan, N., Ravid, R., Dickson, D., Wszolek, Z., Iwatsubo, T., Pickering-Brown, S. M., and Mann, D. M. (2006) *Neuropathol. Appl. Neurobiol.* **32,** 374–387
30. Agarwal-Mawal, A., and Paudel, H. K. (2001) *J. Biol. Chem.* **276,** 23712–23718
31. Head, E., Lott, I. T., Patterson, D., Doran, E., and Haier, R. J. (2007) *J. Alzheimers Dis.* **11,** 61–76
32. Boekhoorn, K., Terwel, D., Biemans, B., Borghgraef, P., Wiegert, O., Ramakers, G. J., de Vos, K., Krugers, H., Tomiyama, T., Mori, H., Joels, M., van Leuven, F., and Lucassen, P. J. (2006) *J. Neurosci.* **26,** 3514–3523
33. Jeganathan, S., von Bergen, M., Brutlach, H., Steinhoff, H. J., and Mandelkow, E. (2006) *Biochemistry* **45,** 2283–2293